



Original article

Synthesis of Co–Ni oxide microflowers as a superior anode for hybrid supercapacitors with ultralong cycle life

Ling-Yang Liu^{a,c}, Xu Zhang^c, Hong-Xia Li^c, Bao Liu^c, Jun-Wei Lang^c, Ling-Bin Kong^{a,b,*}, Xing-Bin Yan^{c,**}^a State Key Laboratory of Advanced Processing and Recycling of Non-ferrous Metals, Lanzhou University of Technology, Lanzhou 730050, China^b School of Materials Science and Engineering, Lanzhou University of Technology, Lanzhou 730050, China^c Laboratory of Clean Energy Chemistry and Materials, State Key Laboratory of Solid Lubrication, Lanzhou Institute of Chemical Physics, Chinese Academy of Sciences, Lanzhou 730000, China

ARTICLE INFO

Article history:

Received 30 May 2016

Received in revised form 26 June 2016

Accepted 4 July 2016

Available online 29 July 2016

Keywords:

Li-ion hybrid capacitor

Energy storage device

Co-precipitation method

Cobalt nickel oxide

APDC

Long cycle life

ABSTRACT

Li-ion hybrid capacitors (LIHCs), composing of a lithium-ion battery (LIB) type anode and a supercapacitor (SC) type cathode, gained worldwide popularity due to harmonious integrating the virtues of high energy density of LIBs with high power density of SCs. Herein, nanoflakes composed microflower-like Co–Ni oxide (CoNiO) was successfully synthesized by a simple co-precipitation method. The atomic ratio of as-synthesized CoNiO is determined to be 1:3 through XRD and XPS analytical method. As a typical battery-type material, CoNiO and capacitor-type activated polyaniline-derived carbon (APDC) were used to assemble LIHCs as the anode and cathode materials, respectively. As a result, when an optimized mass ratio of CoNiO and APDC was 1:2, CoNiO//APDC LIHC could deliver a maximum energy density of 143 Wh kg⁻¹ at a working voltage of 1–4 V. It is worth mentioning that the LIHC also exhibits excellent cycle stability with the capacitance retention of ~78.2% after 15,000 cycles at a current density of 0.5 A g⁻¹.

© 2016 Chinese Chemical Society and Institute of Materia Medica, Chinese Academy of Medical Sciences.

Published by Elsevier B.V. All rights reserved.

1. Introduction

Electronics industry has developed for several decades; however, battery duration has become the biggest problem which restricts the development of new technologies. Long working time means greater energy density in energy storage devices, thus countless researches have focused on the searching for the materials with high specific energy density. And for the emerging electric vehicles, energy storage devices not only require high energy density but also high power density and long cycle life. Compared to the conventional lithium-ion batteries (LIBs), supercapacitors (SCs) are considered to be one of the possible replaceable energy storage devices because of their short charge/discharge time, ultrahigh power density and stable cycle life [1–5]. In the past few years, supercapacitor electrode materials

including electrochemical double layer capacitor materials which store energy from ion adsorption/desorption and pseudocapacitor materials which obtain from surface Faradic redox reactions have been received much research attention [6–10]. However, their specific energy densities are still insignificant in comparison with LIBs [11]. Thus, fabricating novel energy storage devices with high energy density and power density as well as long cycle life are urgent needs.

Li-ion hybrid capacitors (LIHCs), composing of a lithium-ion battery type anode and a supercapacitor type cathode, gained worldwide popularity due to their harmonious integrating the virtues of LIBs and SCs according to the high capacity of the energy-type redox anode, the fast charging rate of power-type double-layer cathode and extended working voltage window resulted from using organic electrolytes [12–16]. Recently, lithium pre-intercalation of the carbon has been extensive studied as electrode materials for LIHCs [17], however, carbon anodes usually exhibit low capacity due to the poor ability for storing lithium ions. Therefore, seeking LIHCs anode materials which can effectively storage lithium-ion is still a challenge. Nowadays, many attempts have been made in this area. The reported potential anode

* Corresponding author at: School of Materials Science and Engineering, Lanzhou University of Technology, Lanzhou 730050, China.

** Corresponding author.

E-mail addresses: konglb@lut.cn (L.-B. Kong), xbyan@licp.cas.cn (X.-B. Yan).

materials mainly include $\text{Li}_4\text{Ti}_5\text{O}_{12}$ [18,19], MnO [20], $\text{Li}_2\text{FeSiO}_4$ [21,22], graphene [23,24], lithium pre-intercalated graphite, hard and soft carbon [17,25]. Previous reports have proved that the use of pseudocapacitive materials as LIHCs anode can obtain fast surface process instead of diffusion limited kinetics [26,27]. Nickel and cobalt oxide or sulfide such as NiO , Co_3O_4 and NiS are considered as a typical pseudocapacitive material in aqueous electrolyte, but they are rarely used as anode materials in LIHCs with organic electrolytes [28–30]. And redox reactions between transition metal oxides and lithium ion can provide certain faradaic pseudocapacitance for LIHCs [16,31]. Wang and his co-workers reported a flower-like $\text{Co}(\text{OH})_2$ as the anode materials in aqueous hybrid supercapacitors. The $\text{Co}(\text{OH})_2$ anode coupled with VN cathode assembled hybrid supercapacitors delivered an energy density of 22 Wh kg^{-1} and an excellent rate capability [17]. However, a cobalt–nickel double oxide, as a typical cobalt oxide and nickel oxide with ultrahigh capacity, has not been studied in LIHCs with organic electrolytes.

In this paper, Co–Ni oxide (CoNiO) was successfully synthesized via a simple co-precipitation method and followed annealing in air. As-prepared sample exhibits a microflower-like morphology composed of thin nanoflakes. And the atomic ratio of as-synthesized CoNiO is determined to be 1:3 through XRD and XPS analytical method. As a typical battery-type material, CoNiO and capacitor-type activated polyaniline-derived carbon (APDC) were used to assemble LIHCs as the anode and cathode electrode materials, respectively. As a result, when an optimized mass ratio of CoNiO and APDC was 1:2, CoNiO//APDC LIHC could deliver a maximum energy density of 143 Wh kg^{-1} at a working voltage of 1–4 V. It is worth mentioning that the LIHC also exhibits excellent cycle stability with the capacitance retention of $\sim 78.2\%$ after 15,000 cycles at a current density of 0.5 A g^{-1} .

2. Experimental

2.1. Synthesis of Co–Ni oxide nanoflakes and activated polyaniline-derived carbon nanorods

All of the chemicals were of analytical grade and were used without further purification. CoNiO were synthesized by a facile chemical co-precipitation method followed by a simple calcinations process. First, a mixed aqueous solution of 1 mol L^{-1} $\text{NiCl}_2 \cdot 6\text{H}_2\text{O}$ and 1 mol L^{-1} $\text{CoCl}_2 \cdot 6\text{H}_2\text{O}$ was made, the molar ratios of the $\text{NiCl}_2 \cdot 6\text{H}_2\text{O}:\text{CoCl}_2 \cdot 6\text{H}_2\text{O}$ was 3:1. The pH value of the mixed solution was slowly adjusted to 9 by adding slowly 5 wt% $\text{NH}_3 \cdot \text{H}_2\text{O}$ at room temperature. The resulting suspension was kept stirring at this temperature for 3 h. Then the solid was filtered, washed with distilled water several times, and annealed in air at $250 \text{ }^\circ\text{C}$ for 6 h.

The polyaniline (PANI) nanorods were synthesized by oxidative polymerization of aniline with ammonium per-sulfate in an aqueous solution containing citric acid. A typical process was shown as follows: 10 g of aniline and 10 g of citric acid were mixed in 1000 ml of distilled water. Then, an aqueous solution of ammonium persulfate was rapidly added into the above mixture solution with a vigorous stirring. After 30 s, the stirring was stopped and the resulting solution was left standing for 24 h at $4 \text{ }^\circ\text{C}$ in a refrigerator. After that, a dark green PANi nanorods suspension with high suspended stability was formed. The PANi nanorods were collected by filter with water and then dried in freezer dryer for 48 h. As-prepared PANi nanorods were then pyrolyzed at $800 \text{ }^\circ\text{C}$ for 1 h under argon atmosphere to obtain PANi-derived carbon (denoted as PDC). Subsequently, KOH activation was carried out as follows. Typically, 0.4 g of PDC was impregnated with 2.4 g of KOH in aqueous phase with the aid of sonication. After removal of water,

the dried PDC/KOH mixture was heated at $800 \text{ }^\circ\text{C}$ for 1 h under an argon atmosphere. After being cooled down to room temperature, the product was washed with dilute HCl solution and ultrapure water until the pH value of the washing water reached 7, and then dried at $60 \text{ }^\circ\text{C}$ in air. The final porous activated PDC nanorods product was designated as APDC.

2.2. Fabrication of half-cell and hybrid device

All the supercapacitor devices studied for the material performance in this work were fabricated using the two-electrode standard method.

For fabrication of CoNiO composite electrode, 80 wt% of active material CoNiO, 10 wt% of acetylene black as the conducting filler, and 10 wt% of polyvinylidene fluoride (PVDF) in methyl-2-pyrrolidone (NMP) were well mixed and then coated on the copper foil which served as a current collector. After heated at $110 \text{ }^\circ\text{C}$ for 10 h under vacuum, the sheet was pressed and finally the electrode was obtained. For the cathode materials APDC, 90 wt% APDC and 10 wt% polytetrafluoroethylene (PTFE) were mixed and then coated on the aluminum foil. After heated at $110 \text{ }^\circ\text{C}$ for 10 h under vacuum, the electrode was pressed, and also the cathode electrode was obtained. The diameters of the copper foil and aluminum foil are both 1.2 cm.

For half cells, both anode and cathode were tested using coin type cells (2032), where Li metal foil was used as the counter and reference electrode, and 1 M LiPF_6 dissolved in 1:1 v/v mixture of ethylene carbonate/diethyl carbonate (EC/DEC) was employed as the electrolyte. Li-ion hybrid capacitors were also assembled in coin cells with pre-activated CoNiO anode (charged–discharged for 10 cycles and ending in a lithiated state at 0.01 V under a low current density of 0.1 A g^{-1}) and APDC cathode in the same electrolyte, and the optimized mass ratio of anode/cathode was 1:2.

2.3. Characterization and electrochemical measurement

The microstructure of CoNiO and APDC were investigated by a field-emission scanning electron microscope (FESEM, JSM-6701F) and transmission electron microscope (TEM, JEOL 2100 FEG). The surface elemental distribution, crystal structure and specific surface area of CoNiO were characterized by X-ray diffraction (XRD, TTR-III), X-ray photoelectron spectroscopy (XPS, ESCA-LAB250xi) and Brunauer-Emmett-Teller method (BET, Micromeritics ASAP 2020).

The electrochemical performances of the cathode electrode, anode electrode and hybrid supercapacitors were investigated by cyclic voltammetry (CV), galvanostatic charge/discharge (GCD) and electrochemical impedance spectroscopy (EIS) using a Chi660d electrochemical workstation (CHI Instruments, China). CV studies of CoNiO Li-half battery were carried out on were carried out using Autolab 302N (Co., Switzerland Metrohm). The cycling life tests were performed on a LAND system (CTA2001A, Wuhan Land Electronic Co., Ltd.). Electrochemical impedance spectroscopy (EIS) test was conducted at frequency from 0.01 Hz to 0.1 MHz.

The specific capacitance of the electrodes and the supercapacitor devices is concluded using Eq. (1):

$$C_m = \frac{i \times t}{m \times (V_{\max} - V_{\min})} \quad (1)$$

where C_m (F g^{-1}) is the specific capacitance, i (A) is the discharge current, t (s) is the discharge time, m (g) is the loading mass of single electrode or total mass of two electrodes in hybrid supercapacitor, V_{\max} and V_{\min} is the maximum and minimum potential of single electrode or work voltage of LIHCs.

The specific energy density and power density of the hybrid supercapacitors are concluded by Eqs. (2) and (3) based on GCD curves:

$$E = \frac{1}{2} \times C \times (V_{\max}^2 - V_{\min}^2) \quad (2)$$

$$P = \frac{E}{t} \quad (3)$$

where E (Wh kg⁻¹) is the specific energy density, C (F g⁻¹) is the specific capacitance, V_{\max} and V_{\min} are the maximum and minimum work voltage applied, P (W kg⁻¹) is the specific power density and t (s) is the discharge time.

3. Results and discussion

3.1. Fabrication and characterization

Fig. 1 shows the fabrication procedure of CoNiO. The CoNiO was prepared by a simple co-precipitation method using CoCl₂·6H₂O and NiCl₂·6H₂O as precursor. After annealing at a low temperature of 250 °C in air, CoNiO can be successfully obtained while the molar ratio of the cobalt and nickel precursor in mixed solution was 1:3. [32] The atomic percentage of the elements Co and Ni in CoNiO was determined based on the results of XPS. Fig. S1a in Supporting information is the XRD pattern of the CoNiO which is in agreement with the JCPDS card: 01-1239 of NiO and JCPDS card: 01-1227 of CoO. This result shows that as-synthesized sample was composed of NiO and CoO with the same attice structure. The low-magnification scanning electron microscope (SEM) image in Fig. 2a clearly shows that the as-synthesized CoNiO consists of microflowers with diameter of ~0.4 μm, and insert of Fig. 2b reveals that these microflowers are composed of interconnected nanoflakes. The thickness of these nanoflakes is ~20 nm. The TEM image of CoNiO in Fig. S1b shows the typical nanoflakes composed microfalowers morphology, and the thickness of the nanoflakes is close to result from SEM images. These microflowers with thin nanoflakes are beneficial to the infiltration of the electrolyte and provide larger specific surface area. This porous structure was also certified by Nitrogen adsorption–desorption data in Fig. 2b. The pore size distribution in inset of Fig. 2b explained the existence of mesoporous (3–50 nm) and small macroporous (~100 nm) in CoNiO. The Brunauer-Emmet-Teller (BET) specific surface area of

as-synthesized CoNiO is calculated to be ~112.5 m² g⁻¹ with a large pore volume of ~0.30 cm³ g⁻¹. Such porous structure of CoNiO could benefit the penetration of the electrolyte, which is essential for surface redox reactions.

Moreover, as seen in Fig. 2c–f, XPS analyses further show the distribution of element and the valence state of the Ni and Co in CoNiO sample. As shown in Fig. 2c, irrelevant elements does not exist in the survey XPS spectrum of the CoNiO sample. Also, insert table in Fig. 2c shows that the atom percent of Co and Ni in our sample were ~5.84% and ~15.1%. That is to say, the atom ratio of Co and Ni is ~1:3, and this is in agreement with the elements ratio in precursor used in preparing the sample. A high-resolution XPS spectrum for the Ni 2p peak is shown in Fig. 2d. Spin-orbit Ni 2p^{1/2} and Ni 2p^{3/2} peaks are located at 873.10 eV and 855.43 eV, and the corresponding satellite is located at 879.16 eV and 861.40 eV. The binding energy separation between main peak and satellite peak both is ~6 eV, indicating the nature of Ni²⁺, and this is the same with the other reported NiO [33–36]. A high-resolution XPS spectrum for the Co 2p peak is also exhibited in Fig. 2e. Spin-orbit Co 2p^{1/2} and Co 2p^{3/2} peaks are located at 796.31 and 780.75 eV, and the corresponding satellite is located at 802.47 eV and 786.69 eV. The spin-orbit of Co 2p demonstrates the existence of Co²⁺, and this is also the same with the other reported CoO [37–39]. The pattern of O 1s spectrum in Fig. 2f can be separated into three parts, suggesting the presence of three types of oxygen-containing species. The bands at 529.67 eV and 531.26 eV can be retrieved as the oxygen bonds of O–Ni and O–Co, respectively [40–42]. And the band at higher binding energy of 532.7 should be the–OH in the sample.

3.2. Electrochemical performance

The capacity of the CoNiO in Li-half cells was firstly explored. The charge storage behaviour was characterized by cyclic voltammetry. Fig. S2a in Supporting information shows the first three CV cycles of a new coin cell at a scan rate of 0.1 mV s⁻¹. The strong peak at 0.53 V indicated the forming of the SEI (Solid electrolyte interphase), and this peak disappeared at second and third cycle which states that the SEI formed completely at first cycle. The reduction peak at 1.07 V at first cycle moved to 0.92 V at second cycle and 0.90 V at third cycle and this peaks turn stable at the following cycles. The almost coincident curves and synchronized peaks of the second and third cycle suggested good cycle

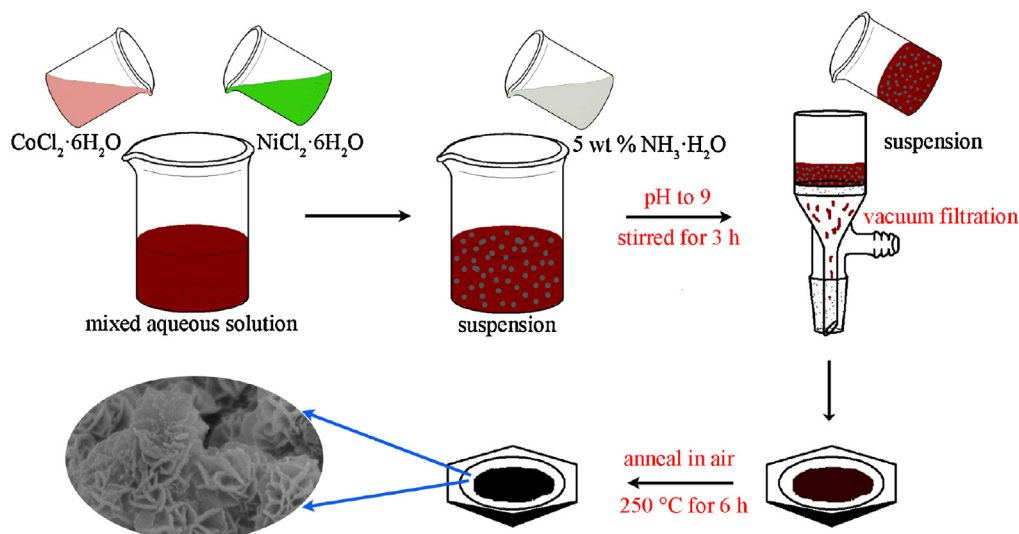


Fig. 1. Schematic illustrations of the fabrication procedure for the CoNiO.

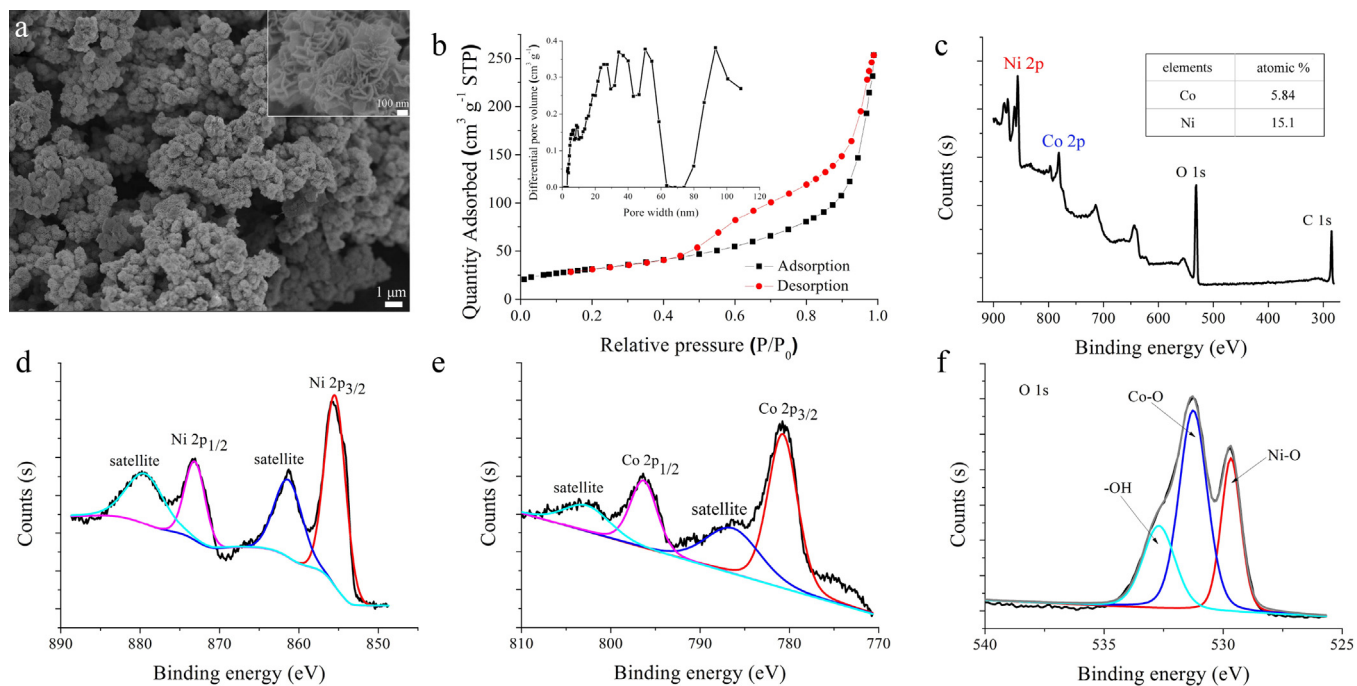


Fig. 2. (a) SEM image of CoNiO (high-magnification SEM image in inset). (b) N_2 adsorption–desorption isotherms of CoNiO. Insert is the pore size distribution. XPS spectra: (c) survey (atom ratio of Co and Ni in insert table), (d) Ni 2p, (e) Co 2p and (f) O 1s spectra.

ability of CoNiO in Li-half cells. Fig. S2b is the CV curves at different scan rates. It is noteworthy that with the increase of the scan rates, the areas of peaks are increased, and the location of main peaks remain unmoved. The CoNiO presents an impressively large-current cycling performance, where a capacity of 251.9 mAh g^{-1} can be maintained for 1200 cycles at 1 A g^{-1} (Fig. S2c). The Nyquist plots before and after cycles were shown in Fig. S2d. During cycle process the CoNiO materials changed into Co–Ni alloys, thus the alternating current impedance decreases after 1200 cycles. These results suggested that the as-prepare CoNiO possess high capacity and excellent cycle performance, and it is suitable for the LIHCs as an superior anode material.

Cathode materials in LIHCs are usually activated carbon materials because of their low cost, large surface area and physical and chemical stability ($>4.5 \text{ V}$ vs. Li^+/Li) [12,43,44]. In our work, activated polyaniline derived carbon (APDC) was prepared by carbonization of the polyaniline nanorod and followed by KOH activation (more details seen experimental part or in our previous work) [16,45]. SEM image and transmission electron microscopy (TEM) image of APDC in Fig. S3 in Supporting information both show the nanorod morphology. Porous structure is clearly shown in the high-magnification TEM image in insert of Fig. S3b. The porous nanorods structure will also benefit the diffusion and transport of electrolyte ions during the fast charge/discharge reaction. Due to the porous structure of APDC, excellent electrochemical performance of the cathode materials can be obtained.

Fig. S4a in Supporting information shows the CV curves of APDC electrode over $3.0\text{--}4.5 \text{ V}$ (vs. Li^+/Li) with scan rates from 10 to 100 mV s^{-1} , and galvanostatic charge/discharge (GCD) curves with different current densities were shown in Fig. S4b. The CV curves are typical rectangular shape and the GCD curves are nearly isosceles triangle, indicating an ideal capacitive behavior of EDLC. The APDC electrode exhibits high specific capacitance of $\sim 156.3 \text{ F g}^{-1}$ at a current density of 0.5 A g^{-1} . The APDC remained 64.5% of the initial capacitance when current densities changed from 0.5 to 10 A g^{-1} (Fig. S4c). Fig. S4d was the Nyquist plot of APDC in Li half cells.

Before fabricating a LIHC, anode electrode of CoNiO was pre-activated for 10 cycles at 100 mA g^{-1} in a Li half-cell then lithiated to 0.01 V which was shown in Fig. S5 in Supporting information. After lithiated to 0.01 V , Li^+ will insert into the CoNiO. Then the pre-activated CoNiO anode and APDC cathode are employed to fabricate a Li-ion hybrid capacitor (CoNiO//APDC LIHC). In order to obtain the best electrochemical performance of the LIHCs, fine tuning of the mass ratio of CoNiO to APDC was firstly determined. The ratios are 3:1, 2:1, 1:1, 1:2 and 1:3. CV curves of CoNiO//APDC LIHC with different mass ratios at the voltage window of $1\text{--}4 \text{ V}$ are shown in Fig. S6a in Supporting information. Because of integrating a lithium-ion battery type anode and a supercapacitor type cathode, the shapes of CV curves are little different from the CV shapes of lithium-ion battery and supercapacitor. However, CV shapes of CoNiO//APDC LIHC are more like the CV shapes of supercapacitor due to the reservation of the fast ion transport and reaction of supercapacitors. With the increase of the ratio, CV curves areas increased until the ratio turns to 1:2, and the CV shape was closest with rectangle. Fig. S6b was the GCD curves at current density of 0.1 A g^{-1} . The highest specific capacitance is 68.6 F g^{-1} when the mass ratio reaches 1:2. The electrochemical performance of the CoNiO//APDC LIHC are the best while the mass ratio of the CoNiO anode and APDC cathode was 1:2 which is in good agreement with results of CV curves. Fig. S6c was the rate performance of the LIHCs with different ratios. Fig. S6d was the Nyquist plots of the LIHCs with different ratios. The intercept on the Z real axis is the equivalent series resistance (ESR) which is composed of the internal resistance of current collector, electrolyte, active material and the connect resistance between current collector and active material [46]. With the increase of mass ratios, the ESR decreases because of the better conductivity of APDC. The response in low-frequency range reflects the diffusion impedance of the LIHCs. The diffusion impedance decreases while the mass ratios increased, and it turns the least when the ratio is 1:2. However, when the mass ratio reaches 1:3, the diffusion impedance increases. This is probably because the APDC become thicker on current collector, and thicker APDC may result in hard infiltration with electrolyte. The Nyquist results are in good

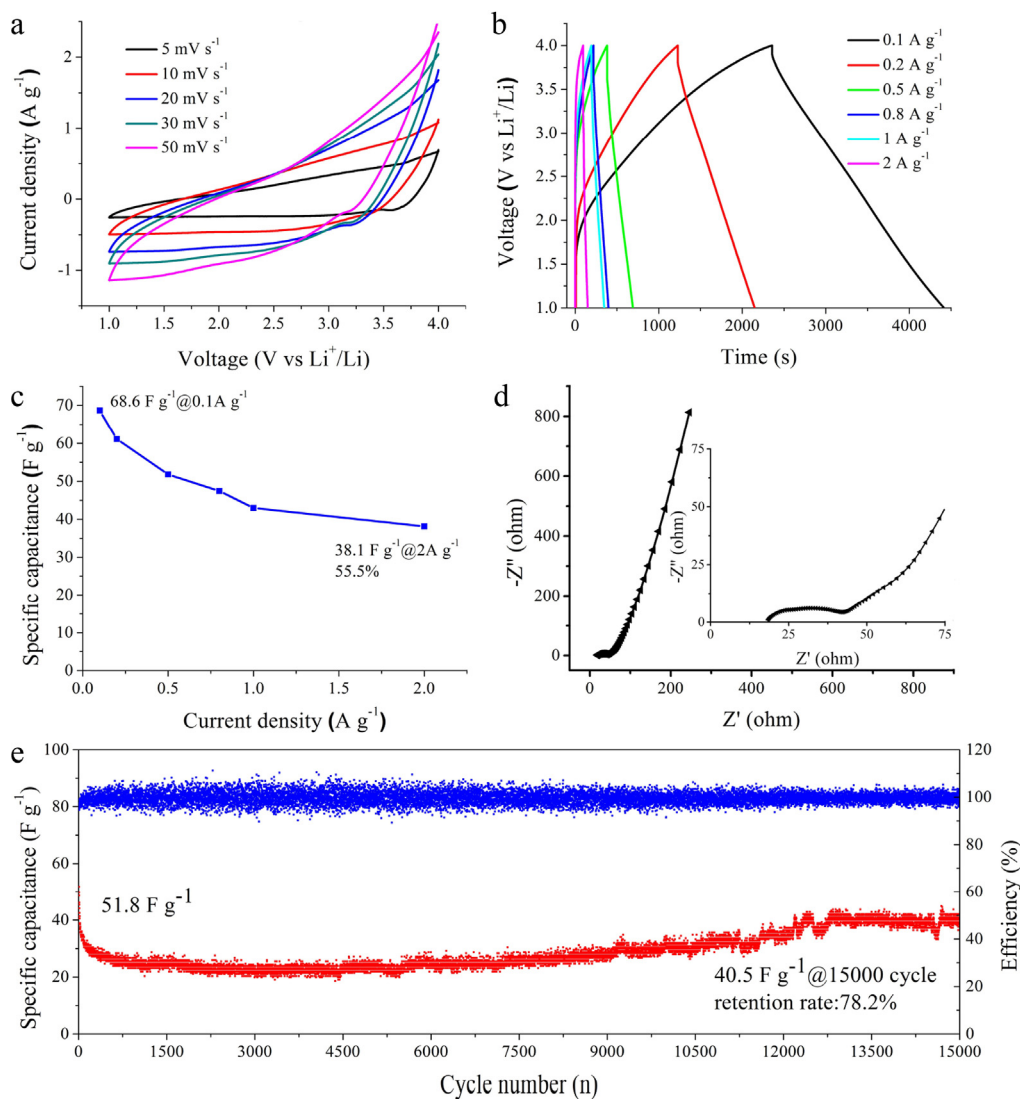


Fig. 3. Electrochemical performance of the LIHC with the mass ratio of 1:2. (a) CV curves at different scan rates from 5 mV s⁻¹ to 50 mV s⁻¹ with a voltage window of 1–4 V. (b) GCD curves at current densities from 0.1 A g⁻¹ to 2 A g⁻¹. (c) Rate performance. (d) Nyquist plot. Insert is the high-magnification image at high frequency. (e) Cycle performance of the LIHC at a current density of 0.5 A g⁻¹.

agreement with the CV and GCD curves. Via these comparisons of the electrochemical performance, the best mass ratio of anode materials CoNiO and cathode materials APDC is 1:2.

As a result, mass ratio of 1:2 was chosen to assemble the LIHCs and these LIHCs were carefully studied. CV curves at different scan rates from 5 mV s⁻¹ to 50 mV s⁻¹ of CoNiO//APDC LIHC were displayed in Fig. 3a. The CV shapes are near rectangle, indicating the rapid reaction of the as-assembled LIHC. GCD curves with current densities from 0.1 A g⁻¹ to 2 A g⁻¹ in Fig. 3b were approximately linear slope. These shapes of GCD curves indicated that the CoNiO//APDC LIHC we assembled maintained the fast charge–discharge property of supercapacitors. The CoNiO//APDC LIHC demonstrated a specific capacitance of 68.6 F g⁻¹ at current density of 0.1 A g⁻¹. When current density reaches to 2 A g⁻¹ which is 20 times larger, the specific capacitance still maintained 38.1 F g⁻¹. Fig. 3d is the Nyquist plot of the LIHC, the ESR is ~18.4 Ω which is low in LIHCs, and also is the diffusion impedance. This extremely low impedance of LIHCs with mass ratio of 1:2 developed the electrochemical performance. Furthermore, CoNiO//APDC LIHC also exhibits an excellent cycle stability with the capacity retention of ~78.2% after 15 000 cycles at a current density of 0.5 A g⁻¹ which was shown in Fig. 3e. The specific

capacitance dropped abruptly to 30.4 F g⁻¹ after first 100 cycles, and the values came to 21.9 F g⁻¹ slowly after 4000 cycles. After these decrease stages, the specific capacitance raised slowly until 15,000 cycles. At the first several thousand cycles, CoNiO transformation and active materials activation occurred and the active materials should not be used completely. After the transformation and the activation finished (approximate 5000 cycles), the active materials became activated and the use efficiency became higher. Thus, the specific capacitance is increasing. The specific capacitance finally maintained 40.5 F g⁻¹ after ultralong cycles, and our result is commendable as far as we know. In addition we compared our result with other reported values in Table 1.

The Ragone plots of CoNiO//APDC LIHC is shown in Fig. 4, and Ragone plots of the CoNiO//APDC LIHCs with different mass ratios were shown in Fig. S7 in Supporting information. We also compared our results with other reported LIHCs [19,44,47]. At a power density of 250 W kg⁻¹, CoNiO//APDC LIHC can achieve a high energy density of ~143 Wh kg⁻¹, which is higher than symmetric APDC//APDC supercapacitor (~60 Wh kg⁻¹) and other reported LIHCs. Even at a high power density of 5 kW kg⁻¹, CoNiO//APDC LIHC can still deliver energy density of ~79.4 Wh kg⁻¹.

Table 1
Comparison of the cycle performance of various reported LIHCs.

LIHCs	Cycle number	Current density	Retention rates	References
VN-RGO//APDC	1000	2 A g ⁻¹	83%	[16]
MnO-C//AC	3500	4 A g ⁻¹	92.5%	[20]
Si/C//NAC	8000	1.6 A g ⁻¹	76.3%	[43]
Li ₄ Ti ₅ O ₁₂ //KC21-900	10,000	1 A g ⁻¹	76%	[44]
NiCo ₂ O ₄ //AC	2000	0.3 A g ⁻¹	100%	[47]
CoNiO//APDC	15,000	0.5 A g ⁻¹	78.2%	Our work

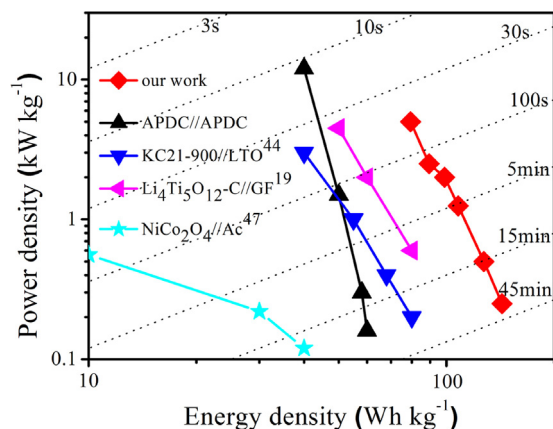


Fig. 4. Ragone plot of the CoNiO//APDC LIHC with mass ratio of 1:2 and APDC//APDC symmetric supercapacitor. The energy and power densities are compared with other reported LIHCs: Li₄Ti₅O₁₂-C//Graphene form [19], KC21-900//LTO [44], NiCo₂O₄//AC [47].

The superior electrochemical performance of CoNiO//APDC LIHC can be attributed to the following aspects: Firstly, CoNiO anode is a typical pseudocapacitive material with high capacitance and a wide working potential (0.01–3 V) in lithium-ion battery. The excellent cycle performance of Li-half cells also confirms the ultralong cycle performance in CoNiO//APDC LIHCs. Secondly, the hierarchical porous structure of CoNiO provides more surface area for approaching of the electrolyte ions and fast charge transfer between electrode and electrolyte. Larger specific area and porous structure may avail the morphology stabilization which can also improve the cycle ability in LIHCs. Lastly, the APDC cathode with high surface area confirms the rapid Li ions adsorption/desorption and also provides the passways for transport of the electrolyte ions. The enduring carbon cathode with firm structure can help to strengthen the electrochemical ability of the LIHCs, especially the cycle performance. These three advantages ensured outstanding electrochemical properties of CoNiO//APDC LIHCs.

4. Conclusion

Co-precipitation method has been used to synthesis CoNiO composites. The microscopic structure and feature properties of the composites are characterized by XRD, SEM, TEM, XPS and N₂ adsorption-desorption. The CoNiO composites are assembled into lithium ion half batteries with lithium foil to charge–discharge ten times for implanting Li⁺ into the as-prepared composites, and the pre-intercalation CoNiO was used to assemble LIHCs as the anode electrode materials coupled with the APDC cathode. The electrochemical results suggest that the best mass ratio of CoNiO and the APDC is 1:2. The specific capacitance of CoNiO//APDC LIHCs was up to 68.65 F g⁻¹ at a current density of 0.1 A g⁻¹ with voltage window of 1–4 V. The LIHCs can also exhibit a high energy density of ~143 Wh kg⁻¹ at a power density of 250 W kg⁻¹ which was

higher than most of the supercapacitors. Furthermore, CoNiO//APDC LIHC also exhibits an excellent cycle stability with the capacity retention of ~78.2% after 15,000 cycles at a current density of 0.5 A g⁻¹. In conclusion, the CoNiO//APDC LIHCs we assembled with such excellent performance were competent to the next generation energy storage devices.

Acknowledgment

This work was supported by the National Nature Science Foundations of China (Nos. 21573265 and 51501208).

Appendix A. Supplementary data

Supplementary data associated with this article can be found, in the online version, at <http://dx.doi.org/10.1016/j.ccl.2016.07.027>.

References

- Y.Q. Chen, X.N. Zhang, Z.P. Xie, Flexible nitrogen doped SiC nanoarray for ultrafast capacitive energy storage, *ACS Nano* 9 (2015) 8054–8063.
- L. Kang, S.X. Sun, L.B. Kong, J.W. Lang, Y.C. Luo, Investigating metal-organic framework as a new pseudo-capacitive material for supercapacitors, *Chin. Chem. Lett.* 25 (2014) 957–961.
- J.J. Cai, L.B. Kong, J. Zhang, Y.C. Lou, L. Kang, A novel polyaniline/mesoporous carbon nano-composite electrode for asymmetric supercapacitor, *Chin. Chem. Lett.* 21 (2010) 1509–1512.
- M.H. Yu, Y. Zeng, Y. Han, et al., Valence-optimized vanadium oxide supercapacitor electrodes exhibit ultrahigh capacitance and super-long cyclic durability of 100,000 cycles, *Adv. Funct. Mater.* 25 (2015) 3534–3540.
- M.J. Shi, S.Z. Kou, B.S. Shen, et al., Improving the performance of all-solid-state supercapacitors by modifying ionic liquid gel electrolytes with graphene nanosheets prepared by arc-discharge, *Chin. Chem. Lett.* 25 (2014) 859–864.
- G.P. Wang, L. Zhang, J.J. Zhang, A review of electrode materials for electrochemical supercapacitors, *Chem. Soc. Rev.* 41 (2012) 797–828.
- H.W. Wang, Z.A. Hu, Y.Q. Chang, et al., Design and synthesis of NiCo₂O₄-reduced graphene oxide composites for high performance supercapacitors, *J. Mater. Chem.* 21 (2011) 10504–10511.
- D. Chen, Q.F. Wang, R.M. Wang, G.Z. Shen, Ternary oxide nanostructured materials for supercapacitors: a review, *J. Mater. Chem. A* 3 (2015) 10158–10173.
- M. Huang, F. Li, F. Dong, Y.X. Zhang, L.L. Zhang, MnO₂-based nanostructures for high-performance supercapacitors, *J. Mater. Chem. A* 3 (2015) 21380–21423.
- Y.F. An, Z.G. Hu, B.S. Guo, et al., Electrodeposition of honeycomb-shaped NiCo₂O₄ on carbon cloth as binder-free electrode for asymmetric electrochemical capacitor with high energy density, *RSC Adv.* 6 (2016) 37562–37573.
- K.L. Van Aken, M. Beidaghi, Y. Gogotsi, Formulation of ionic-liquid electrolyte to expand the voltage window of supercapacitors, *Angew. Chem. Int. Ed.* 54 (2015) 4806–4809.
- D.P. Dubal, O. Ayyad, V. Ruiz, P. Gómez-Romero, Hybrid energy storage: the merging of battery and supercapacitor chemistries, *Chem. Soc. Rev.* 44 (2015) 1777–1790.
- W. Zhang, Y.H. Qu, L.J. Gao, Performance of PbO₂/activated carbon hybrid supercapacitor with carbon foam substrate, *Chin. Chem. Lett.* 23 (2012) 623–626.
- Z.A. Zhang, M.G. Deng, B.H. Wang, Y.D. Hu, B.C. Yang, Electrochemical hybrid capacitor, *Batt. Bim.* 34 (2004) 295–297.
- L. Zhou, H. Zhang, W.J. Qie, Progress in electrochemical hybrid capacitors, *Chin. J. Power Sources* 37 (2013) 2073–2076.
- R.T. Wang, J.W. Lang, P. Zhang, Z.Y. Lin, X.B. Yan, Fast and large lithium storage in 3D porous VN nanowires-graphene composite as a superior anode toward high-performance hybrid supercapacitors, *Adv. Funct. Mater.* 25 (2015) 2270–2278.
- J. Zhang, X.F. Liu, J. Wang, J. Shi, Z.Q. Shi, Different types of pre-lithiated hard carbon as negative electrode material for lithium-ion capacitors, *Electrochim. Acta* 187 (2016) 134–142.
- L. Deng, W.H. Yang, S.X. Zhou, J.T. Chen, Effect of carbon nanotubes addition on electrochemical performance and thermal stability of Li₄Ti₅O₁₂ anode in commercial LiMn₂O₄/Li₄Ti₅O₁₂ full-cell, *Chin. Chem. Lett.* 26 (2015) 1529–1534.
- L. Ye, Q.H. Liang, Y. Lei, et al., A high performance Li-ion capacitor constructed with Li₄Ti₅O₁₂/C hybrid and porous graphene macroform, *J. Power Sources* 282 (2015) 174–178.
- C.F. Liu, C.K. Zhang, H.Q. Song, et al., Mesocrystal MnO cubes as anode for Li-ion capacitors, *Nano Energy* 22 (2016) 290–300.
- Y. Xu, Y.J. Li, S.Q. Liu, H.L. Li, Y.N. Liu, Nanoparticle Li₂FeSiO₄ as anode material for lithium-ion batteries, *J. Power Sources* 220 (2012) 103–107.
- D. Enslin, M. Stjern Dahl, A. Nyten, T. Gustafsson, J.O. Thomas, A comparative XPS surface study of Li₂FeSiO₄/C cycled with LiTFSI- and LiPF₆-based electrolytes, *J. Mater. Chem.* 19 (2009) 82–88.

- [23] Y.F. Ma, H.C. Chang, M. Zhang, Y.S. Chen, Graphene-based materials for lithium-ion hybrid supercapacitors, *Adv. Mater.* 27 (2015) 5296–5308.
- [24] L.W. Zhao, H.J. Li, M.J. Li, et al., Lithium-ion storage capacitors achieved by CVD graphene/TaC/Ta-wires and carbon hollow spheres, *Appl. Energy* 162 (2016) 197–206.
- [25] Y.G. Lim, M.S. Park, K.J. Kim, et al., Incorporation of conductive polymer into soft carbon electrodes for lithium ion capacitors, *J. Power Sources* 299 (2015) 49–56.
- [26] R.Z. Li, Y.M. Wang, C. Zhou, et al., Carbon-stabilized high-capacity ferroferric oxide nanorod array for flexible solid-state alkaline battery-supercapacitor hybrid device with high environmental suitability, *Adv. Funct. Mater.* 25 (2015) 5384–5394.
- [27] V. Aravindan, J. Gnanaraj, Y.S. Lee, S. Madhavi, Insertion-type electrodes for nonaqueous Li-ion capacitors, *Chem. Rev.* 114 (2014) 11619–11635.
- [28] Z.A. Hu, Y.L. Xie, Y.X. Wang, et al., Synthesis and electrochemical characterization of mesoporous $\text{Co}_x\text{Ni}_{1-x}$ layered double hydroxides as electrode materials for supercapacitors, *Electrochim. Acta* 54 (2009) 2737–2741.
- [29] Y.M. Chen, Z. Li, X.W. Lou, General formation of $\text{M}_x\text{Co}_{3-x}\text{S}_4$ ($\text{M} = \text{Ni, Mn, Zn}$) hollow tubular structures for hybrid supercapacitors, *Angew. Chem. Int. Ed.* 54 (2015) 10521–10524.
- [30] W.D. Yu, W. Lin, X.F. Shao, et al., High performance supercapacitor based on $\text{Ni}_3\text{S}_2/\text{carbon}$ nanofibers and carbon nanofibers electrodes derived from bacterial cellulose, *J. Power Sources* 272 (2014) 137–143.
- [31] Z.M. Zheng, P. Zhang, X.B. Yan, Progress in electrode materials for lithium ion hybrid supercapacitors, *Chin. Sci. Bull.* 31 (2013) 3115–3123.
- [32] J.W. Lang, L.B. Kong, M. Liu, Y.C. Luo, L. Kang, $\text{Co}_{0.56}\text{Ni}_{0.44}$ oxide nanoflake materials and activated carbon for asymmetric supercapacitor, *J. Electrochem. Soc.* 157 (2010) A1341–A1346.
- [33] J.Y. Cheng, B. Zhao, W.K. Zhang, et al., High-performance supercapacitor applications of NiO-nanoparticle-decorated millimeter-long vertically aligned carbon nanotube arrays via an effective supercritical CO_2 -assisted method, *Adv. Funct. Mater.* 25 (2015) 7381–7391.
- [34] S.X. Wu, K.S. Hui, K.N. Hui, K.H. Kim, Ultrathin porous NiO nanoflake arrays on nickel foam as an advanced electrode for high performance asymmetric supercapacitors, *J. Mater. Chem. A* 4 (2016) 9113–9123.
- [35] Y. Bai, M.M. Liu, J. Sun, L. Gao, Fabrication of Ni–Co binary oxide/reduced graphene oxide composite with high capacitance and cyclability as efficient electrode for supercapacitors, *Ionics* 22 (2016) 535–544.
- [36] Q. Li, Q. Wei, L.J. Xie, et al., Layered NiO/reduced graphene oxide composites by heterogeneous assembly with enhanced performance as high-performance asymmetric supercapacitor cathode, *RSC Adv.* 6 (2016) 46548–46557.
- [37] F. Yang, J.Y. Yao, F.L. Liu, et al., Ni–Co oxides nanowire arrays grown on ordered TiO_2 nanotubes with high performance in supercapacitors, *J. Mater. Chem. A* 1 (2013) 594–601.
- [38] C.R. Zheng, C.B. Cao, Z. Ali, J.H. Hou, Enhanced electrochemical performance of ball milled CoO for supercapacitor applications, *J. Mater. Chem. A* 2 (2014) 16467–16473.
- [39] M.Y. Yang, F.C. Lv, Z.Y. Wang, et al., Binder-free hydrogenated NiO–CoO hybrid electrodes for high performance supercapacitors, *RSC Adv.* 5 (2015) 31725–31731.
- [40] W.B. Xu, B. Mu, A.Q. Wang, Facile fabrication of well-defined microtubular carbonized kapok fiber/NiO composites as electrode material for supercapacitor, *Electrochim. Acta* 194 (2016) 84–94.
- [41] S.I. Kim, J.S. Lee, H.J. Ahn, H.K. Song, J.H. Jang, Facile route to an efficient NiO supercapacitor with a three-dimensional nanonetwork morphology, *ACS Appl. Mater. Interfaces* 5 (2013) 1596–1603.
- [42] D.N. Lan, Y.Y. Chen, P. Chen, et al., Mesoporous CoO nanocubes @ continuous 3D porous carbon skeleton of rose-based electrode for high-performance supercapacitor, *ACS Appl. Mater. Interfaces* 6 (2014) 11839–11845.
- [43] B. Li, F. Dai, Q.F. Xiao, et al., Nitrogen-doped activated carbon for a high energy hybrid supercapacitor, *Energy Environ. Sci.* 9 (2016) 102–106.
- [44] P. Sennu, H.J. Choi, S.G. Baek, V. Aravindan, Y.S. Lee, Tube-like carbon for Li-ion capacitors derived from the environmentally undesirable plant: *Prosopis juliflora*, *Carbon* 98 (2016) 58–66.
- [45] R.T. Wang, X.B. Yan, Superior asymmetric supercapacitor based on Ni–Co oxide nanosheets and carbon nanorods, *Sci. Rep.* 4 (2014) 3712.
- [46] J. Li, Y.H. Wang, J. Tang, et al., Direct growth of mesoporous carbon-coated Ni nanoparticles on carbon fibers for flexible supercapacitors, *J. Mater. Chem. A* 3 (2015) 2876–2882.
- [47] R. Ding, L. Qi, H.Y. Wang, Porous NiCo_2O_4 as an anode material for 4.5 V hybrid Li-ion capacitors, *RSC Adv.* 3 (2013) 12581–12584.